Water-Gas Shift Reaction Kinetics Over μ-Structured $Pt/CeO_2/Al_2O_3$ Catalysts

G. Germani and Y. Schuurman
Institut de Recherches sur la Catalyse, CNRS, 2 Avenue Albert Einstein, 69626 Villeurbanne, France

DOI 10.1002/aic.10764
Published online January 17, 2006 in Wiley InterScience (www.interscience.wiley.com).

Platinum/ceria/alumina catalysts have been prepared in the microchannels of stainless steel platelets. These catalysts are very active for the water-gas shift reaction between 250–400°C. The use of microreactors as kinetic devices has a clear advantage that the thin catalyst film allows the determination of the intrinsic kinetics even in the case of fast reactions. However, the channel design should be such that plug flow conditions are favored. The kinetics of the water-gas shift reaction, free from internal diffusion limitations, have been studied over thin catalyst layers over a large range of operation conditions. The reaction rate is almost zero-order in carbon monoxide and strongly inhibited by the partial pressure of hydrogen and to a lesser extent to that of carbon dioxide. An overall activation energy of 76.8 ± 2 kJ/mol has been measured. The data are best described by a dual-site mechanism, where platinum provides an adsorption site for carbon monoxide and ceria an adsorption site for water. The rate-determining step involves the formation of a complex between a carboxyl species and a hydroxyl group that decomposes over a free platinum site into carbon dioxide and hydrogen. © 2006 American Institute of Chemical Engineers *AIChE J,* 52: 1806-1813, 2006
Keywords: CO conversion, microreactors, plug flow, reaction mechanism

Introduction

Solid polymer fuel cells (SPFC) also known as proton-exchange membrane (PEM) fuel cells are potential candidates for mobile power applications or small stationary power units. Efficient operation of the PEM fuel cells requires high-purity hydrogen. This hydrogen can be produced from hydrocarbon fuels or alcohols by a reforming step, yielding a mixture of hydrogen, carbon monoxide, carbon dioxide and steam. The carbon monoxide level must be reduced below to levels between 10–50 ppm to avoid poisoning of the fuel cell electrodes.[1] This is generally accomplished in several steps that might include the high- and low-temperature water-gas shift (HT-/LT-WGS), as well as a preferential oxidation step. The WGS converts CO into CO_2 by the reaction with water over a suitable catalyst and provides additional hydrogen

$$CO + H_2O \rightleftarrows CO_2 + H_2 \quad \Delta H^{\varnothing} = -41.1 \text{ kJ/mol}, \Delta G^{\varnothing} = -28.6 \text{ kJ/mol} \quad (1)$$

Two types of catalysts are commonly used in industry: a FeCr based catalyst for HT-WGS and a CuZn catalyst for LT-WGS. Due to the thermodynamic constraint, the reaction is operated at the lowest possible temperatures to achieve high conversions. At these low-temperatures, most catalysts are not very active, thus, leading to large reactor volumes. In view of new applications, such as hydrogen generation for PEM fuel cells, a more active catalyst formula is required for down-scaling the reformer, together with fast response, long catalyst lifetime and nonpyrophoric materials.[2]

Pt/CeO_2 has raised interest for the WGS reaction since the late 1970s, when its good CO conversion activity was discovered during the development of three-way catalysts.[3-6] Different groups have reported that ceria-supported platinum catalysts are more active than alumina supported ones.[7, 8] Recently, the Pt/CeO_2 catalyst has received new interest in the context of

Correspondence concerning this article should be addressed to Y. Schuurman at schuurman@catalyse.cnrs.fr.

fuel cells,[9, 10] as these catalysts are highly active in the range of 250 – 400°C, and they are nonpyrophoric and do not require any pretreatment before use.

Two reaction mechanisms for the WGS reaction over ceria-supported transition metal catalysts have been advocated: one that involves a bidentate formate species formed by the reaction of CO and hydroxyl groups on ceria originally proposed by Shido and Iwasa.[11] The rate-determining step is the reaction of the formate species with a hydroxyl group into hydrogen and a carbonate species. The function of the noble metal is to keep the ceria reduced to enable the formation of hydroxyl groups.

On the other hand, Gorte et al.[9, 14] propose a redox mechanism in which carbon monoxide adsorbed on platinum reacts with oxygen atoms derived from the ceria to form carbon dioxide, through a carbonate species as intermediate. The ceria is reoxidized by water, thus, forming hydrogen.

Very few kinetic studies for the WGS over platinum catalysts are reported in the literature and even less address Pt/ceria catalysts. Lam et al.[18] tested various Langmuir-Hinshelwood models to describe their data over a platinum-alumina fiber catalyst. Grenoble et al.[19] have determined the reaction orders and activation energies for a large number of different catalysts among which Pt/Al_2O_3, Pt/SiO_2 and Pt/C. They observed a strong influence of the support on the catalytic activity and they explained the trend of the activity of the different metals with a bifunctional mechanism involving formic acid as an intermediate species.

Mhadeshwar and Vlachos[20] presented recently a microkinetic model for the WGS over platinum. These authors reduced the very complex model into a one step rate equation and tested it against a limited set of experimental data over Pt/ZrO_2. Wheeler et al.[21] presented a rather similar approach for a Pt/alumina and Pt/ceria catalyst.

This article reports on the development of platinum/ceria/alumina catalysts on stainless steel microstructured platelets for the WGS reaction. Microstructured reactors offer excellent temperature control due to their good thermal conductivity and small dimensions.[22] Moreover, the use of thin washcoat layers of catalysts eliminates the intraparticle diffusion limitations that can occur for fast reactions. Microstructured reactors are, therefore, used more and more frequently for kinetic studies.[23, 24] In our case it offers the double advantage of measuring the intrinsic kinetics on the same catalyst geometry as the one to be used in a full-scale process. Modeling of the kinetic data from the microreactor was performed to find the best model in order to get a better understanding of the reaction mechanism on the one hand and on the other hand to find a rate equation for proper reactor design.

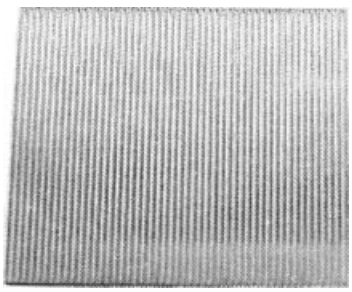

Figure 1. Microstructured platelet containing 49 channels used for the water-gas shift reaction.

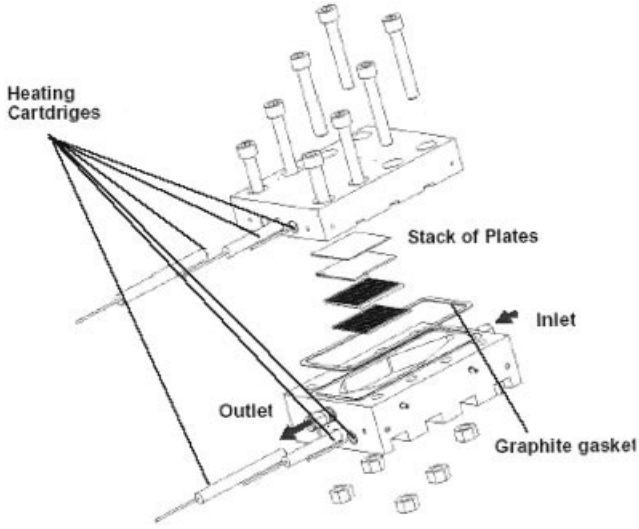

Figure 2. Exploded view of reactor housing with microstructured platelets.

Experimental

Experimental setup

Figure 1 shows a microstructured platelet made of stainless steel having the following dimensions: 50 × 50 × 1 mm, containing 49 channels 400 μm deep and 600 μm wide on only one side of the platelet. The steel grade was ASTM 316Ti (DIN 1.4571). They are placed together with some filler plates (platelets that do not contain any channels) inside a stainless steel housing, shown in Figure 2. The housing pushes down onto the platelets to prevent the gas from passing between the platelets and, thus, assuring that all the gas flows through the channels. The good agreement between the experimental conversions at high temperatures and those calculated according to thermodynamics indicated indeed the absence of any gas bypassing of the catalyst. The housing is sealed with graphite rectangular seals. The inlet section is of a triangular shape that allows a proper gas distribution through the microstructured platelets. The housing can be opened up after reaction, and the platelets can be taken out for analysis purposes. The heating is provided by means of six 500 W heating cartridges inserted into the housing body. The reactor temperature was measured with a thermocouple located in the reactor housing close to the exit. Preliminary measurements showed that the temperature deviation between the inlet and outlet is less than 2°.

Mass-flow controllers regulate the gas flows. Water is dosed by a syringe pump, vaporized and then mixed into the gaseous reactants stream.

The product gas analysis is carried out at the reactor exit by an Inficon Transpector CIS2 mass spectrometer.

Prior to the activity test, each batch of platelets was reduced in a flow of 10% H_2 in argon (total flow = 200 Nml/min). The temperature was raised from 25 to 450°C at a rate of 4°C/min, and then kept at 450°C for 30 min. The reactor temperature is lowered to 200°C in a flow of 10% H_2 in argon. The flow is

then switched to pure argon and subsequently to the reactive flow.

Two, four or six platelets were used for the activity tests. The amount of catalyst deposited on each platelet was about 106 mg on average.

Both carbon and hydrogen balances were established that both amounted to 101 ± 1%. At temperatures above 350°C traces of methane were detected, its concentration amounted to maximum 0.05% at 420°C. In the current article and for all calculations the methane concentration has been neglected.

Catalyst

An aqueous suspension of alumina powder (Alfa Aesar, 3 μm powder) with a commercial type of methylhydroxyethylcellulose binder (Clariant) was prepared. This suspension was used to slurry-coat the channels of the microstructured platelets. All suspension deposited outside the channels was carefully removed. After coating the platelets were calcined at 600°C. The washcoat was then impregnated to incipient wetness with a cerium precursor solution (4.78 wt % Ce^{3+} from $Ce(NO_3)_3 \cdot 6H_2O$, Alfa Aesar: Reaction® 99.5%), using a paintbrush. It was followed by drying and calcination at 400°C for 2 h. The washcoat was then impregnated six times to incipient wetness with a platinum precursor solution (1.17 wt % Pt^{2+} from $Pt(NH_3)_4OH_2$, Alfa Aesar: solution, Pt 8-11% w/w), using a paintbrush. The final catalyst coating was calcined for 10 h at 550°C.

Hydrogen chemisorption

Perrichon et al.[25] developed a method to measure the platinum dispersion of the $Pt/CeO_2/Al_2O_3$ catalysts in powder form. It is based on H_2 chemisorption, and it is performed in a static volumetric apparatus. The powder samples were obtained by carefully scraping part of the washcoat off the microchannels. The samples were pretreated by heating to 573 K *in vacuo*, followed by reduction at 573 K under 13 kPa of hydrogen and evacuation at the reduction temperature. Three reduction cycles were carried out, with 0.5 h duration for each step. This procedure allowed eliminating residual water vapor issued from the reduction and which could be adsorbed on cold parts of the apparatus.

The sample cell was then immersed in a mixture of acetone and solid CO_2, to keep it at a temperature of 195 K. It is necessary to perform hydrogen adsorption at such a low temperature in order to suppress the hydrogen spillover onto the CeO_2.

Two adsorption isotherms are necessary to determine the irreversibly bound chemisorbed hydrogen, which corresponds to the hydrogen adsorbed on the metal surface. The first isotherm gives the total amount of chemisorbed hydrogen. The second isotherm is obtained after evacuating the sample for 15 min treatment at 298 K. The difference between the two isotherms gives the irreversible part of chemisorbed hydrogen. The two isothermal curves were obtained with 5–6 experimental points in the 0.4–5 kPa pressure range, each point being obtained after contacting the catalyst for 10 min with H_2. To calculate the metal dispersion, it was supposed that the adsorption stoichiometry is one hydrogen atom for one surface platinum atom.

Modeling

An integral reactor operation has been used and, therefore, the rate equations have been integrated numerically. A one-dimensional (1-D) homogeneous reactor model has been used.[26] The correctness of this reactor model with respect to the microstructured reactor is discussed in the next paragraph. Since the reaction is stoichiometrically single, the continuity equation for CO is sufficient. The first-order differential equations were numerically integrated using the ODEPACK library.[27] The nonlinear least-square regression analysis has been performed by a Levenberg-Marquardt minimization algorithm.[28,29,30]

Microreactors as kinetic devices

The use of the microstructured reactor as a kinetic device gives some distinct advantages, but a number of precautions have to be taken into account. Proper kinetic experiments ask for ideal reactor behavior. That means well-defined hydrodynamic behavior (for example, plug flow and no by-passing) and absence of mass- and heat- transfer limitations on both channel and pellet scale.

The flow through microchannels with typical diameters of 300 – 1,000 μms is laminar. The fact that this flow can be considered as a plug flow depends on the dispersion coefficient. The value of the dispersion coefficient for this flow will determine the radial and axial concentration profile and is thus a criteria for considering the flow as plug flow.

In the absence of reaction, the dispersion coefficient for fully developed laminar gas flow in cylindrical tubes with a length to diameter ratio greater than 100, and a Reynolds number in the range of 10^{-2} – 100, typical conditions for laboratory tests, is given by the Aris equation[31, 32]

$$D_{Aris} = \frac{u^2 d_t^2}{192D} + D \tag{2}$$

This flow regime is known as the axial dispersion model. In this case the flow can be considered as plug flow if[32]

$$\frac{uL}{D_{Aris}} > 100 \tag{3}$$

In the presence of reaction, Chakraborty and Balakotaiah[33] derive the following equation for the dispersion coefficient, which is modified here according to the Aris equation instead of the Taylor equation

$$D_{reac} = D_{Aris}\left(1 - \frac{d_t^2}{240D} R'(C_m)\right) \tag{4}$$

Reaction at the catalyst on the wall lowers the dispersion coefficient, and, thus, improves the plug flow behavior. The stricter criterion is Eq. 3 with the Aris-dispersion coefficient for nonreactive flow given by Eq. 2. By assuming a molecular-diffusion coefficient of 5 10^{-5} m^2/s for CO[34], and using the above reactor configuration and the conditions listed in Table 1, the lefthand side of Eq. 3 ranges between 150 – 500, thus, satisfying the criteria of plug flow.

Table 1. Investigated Range of Experimental Conditions

Variable	Range
P_{CO}	0.05–0.25 bar
P_{H2O}	0.05–0.4 bar
P_{H2}	0.0–0.45 bar
P_{CO2}	0.0–0.3 bar
Temperature	200–400°C
Flow rate	40–200 ml/min
Catalyst amount	0.21–0.64 g
Total pressure	1.0 bar
W/F_{co}	5.4–220 kg s/mol
CO/H_2O	0.1–2.5
CO conversion	0.02–97%

Using an open housing in which a variable number of platelets are stacked, such as the one used in this study, can lead to bypassing of the gas flow if the platelets or the filler plates have not the exact size. In the initial experiments bypassing was revealed by the fact that the thermodynamic equilibrium was not attained at higher temperatures. By using the proper filler platelets this issue has been solved.

Delsman et al.[35] studied the influence of the variance of channel width, and the variance in catalyst weight on the overall conversion. They showed that for a first-order reaction, both experimentally and theoretically, variations in the amount of catalysts per channel lead to lower conversions. In fact this is analogous to a badly diluted powder catalyst with an inert powder in the case of fixed bed reactors. This can be avoided by carefully selecting platelets with similar amounts of catalyst weights.

Note that the requirements for plug flow conditions, as well as the need for small deviations in the catalyst amount per platelet favor a microstructured reactor design that stacks the platelets in a serial fashion rather than in the commonly encountered parallel layout.

As mentioned previously, the two main advantages of microstructures for kinetic measurements are the excellent thermal conductivity and the thin catalysts layers that are employed. The first lead to better isothermal conditions while the second leads to the absence of internal concentration gradients.

The latter has been demonstrated for the water-gas shift reaction over a $Pt/CeO_2/Al_2O_3$ catalyst[36]. The conversion of CO was measured at various temperatures over both a powder sample with an average particle size of 250 μm, and over the same catalyst washcoated on stainless steel platelets. The equivalent particle diameter of the catalyst layer inside the microchannel was 37 μm. The initial rates obtained at low-temperatures over the powder sample compare well with those obtained over the microstructured platelets. However, the data between powder and platelet deviate substantially at higher temperatures and higher conversion levels. The conversion over the powder samples is lower than that of the platelets indicating that there might be diffusion limitation inside the powder grains. A simulation that took into account the diffusion of matter inside the powder grains, and the reaction rates measured in the microreactor confirmed this.

Results

Characterization

A scanning electron micrograph of the cross section of the washcoat inside a microchannel after slurry coating with the alumina suspension is shown in Figure 3. The picture shows that the washcoat is compact with a U-shaped cross section (black area in Figure 3). Further scanning electron microscopy showed only minor cracks in the washcoat layer. From the micrograph, a maximum washcoat thickness of 39 μm and a minimum thickness of 24 μm has been estimated.

All platelets were weighed after the final calcination, and the washcoat weight was in average 106 mg. By using the dimensions of the washcoat layer from the SEM micrograph and the average weight of washcoat deposition, an alumina washcoat density of 1450 kg/m^3 has been calculated, which is a typical value observed for alumina washcoats on cordierite monoliths.[37] This confirms a homogeneous deposition of the catalyst layer throughout the channels of the microstructured platelet.

Some of the washcoat was scraped off the platelets and used for atomic emission spectroscopy analysis. The measured metal weight percentages are as follows:

0.79 wt % of Pt, 3.40 wt % of Ce, 46.44 wt % of Al.

The specific surface area of the scraped-off catalyst was measured by N_2 adsorption, and compared with the surface of the pure alumina calcined 10h at 600°C. The BET surface area of the pure γ-Al_2O_3 was equal to 82 m^2/g, which decreased to 72 m^2/g after impregnation with ceria and the platinum solution.

A Pt dispersion of 67% was measured according to the procedure proposed by Perrichon et al.[25] The relation between the platinum dispersion and the surface area average diameter, assuming 1.42 10^{19} platinum atoms per square meter is given by Scholten et al.[38]

$$\bar{d}_{Pt} = \frac{1.3}{D_{Pt}} \quad \text{(nm)} \tag{5}$$

Substitution of 0.67 into the above Eq. 5, gives an average particle size diameter of approximately 2 nm.

The $Pt/CeO_2/Al_2O_3$ catalyst was reduced overnight at 350°C, and then replicas were made out of a small sample. Transmission electron microscopy was carried out on the replicas of the catalyst sample in order to increase the contrast between Pt particles, and the background by dissolving the

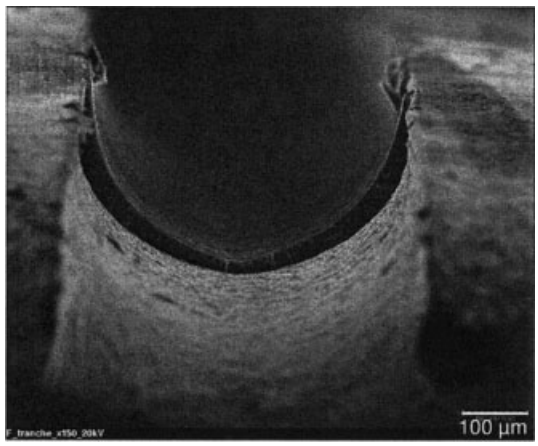

Figure 3. Washcoats in microchannels: channel and washcoat layer cross section.

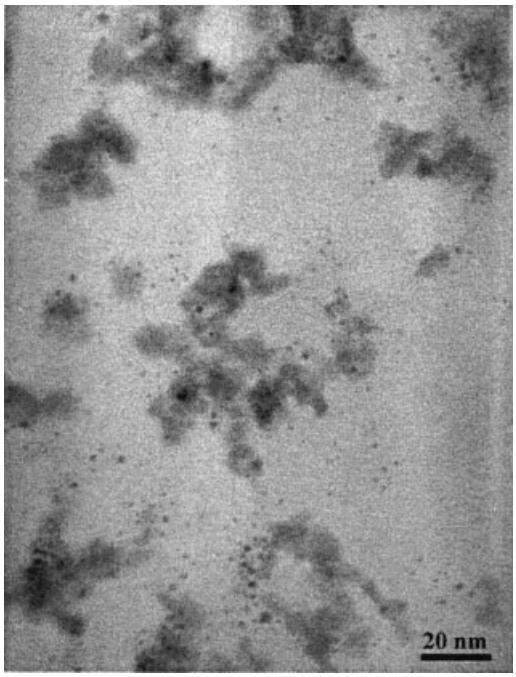

Figure 4. TEM image of replicas of the Pt/ceria/alumina catalyst (the alumina has been removed).

alumina support. This allows a better estimation of Pt particle size, and it also allows observing the platinum distribution over both the ceria and the alumina. An example of such a transmission electron micrograph is shown in Figure 4. The visible species are platinum (black spots) and ceria (dark gray areas). It can be seen that Pt particle size corresponds to the one estimated from the hydrogen adsorption and Eq. 5. The Pt particles are randomly distributed over the entire catalyst surface area, so that only a small fraction of them are deposited on the ceria. This fraction has not been estimated. The micrographs show the presence of both monocrystalline ceria particles as small as 3 nm, as well as much larger polycrystalline particles (~20 –50 nm).

Two types of adhesion tests were performed on the coated platelets. The fall test consisted of dropping the platelets three times on a hard surface from a 50 cm height with the channels facing down, and the weight loss was monitored. No weight loss was recorded for any of the prepared platelets. A more severe test was, therefore, carried out that consisted of exposure to ultrasounds. According to a method described in the patent literature[39] and later used by other authors,[40] the coated platelets were immersed in petroleum ether inside a sealed beaker, and then treated in a sonicator for 30 min (frequency: 42 kHz, RF power: 130W). The largest recorded weight loss was 1.7% of the initial washcoat weight.

Activity tests

Table 1 gives the different ranges of operating conditions that have been used for the kinetic experiments. Close to a hundred experiments were carried out of which 70 where used to establish the rate equation and the parameter estimation. After an initial regression analysis of the data by a power law rate equation the initial rate at the reactor entrance has been

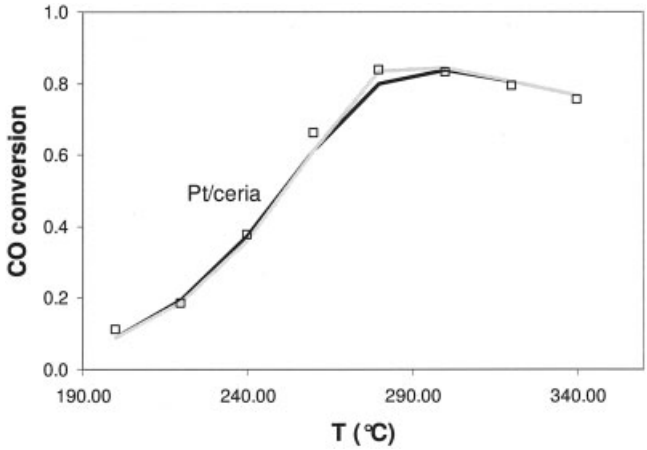

Figure 5. CO conversion as a function of the temperature.

P_{CO} = 0.1 bar, P_{H2O} = 0.2 bar, P_{H2} = 0.3 bar, P_{CO2} = 0.1 bar, balanced in argon, F_{total} = 100 Nml/min, W = 636 mg. (symbols: experimental data, gray line: rate Eq. 6, black line: rate Eq. 9).

calculated. All data with observed rates higher than 0.15 mol/s kg_{cat} were omitted from the final set for regression analysis. This restricted the upper temperature limit to 360°C. The Weisz modulus corresponding to a rate of 0.15 mol/s kg_{cat}, assuming an irreversible zero-order reaction for the disappearance of CO, was calculated to be equal to 0.3, corresponding to an effectiveness factor of 0.95.[41] However, the large majority of the experimental data corresponded to rates in the range of $1\ 10^{-3} - 5\ 10^{-2}$ mol/s kg_{cat}. Hence, diffusion limitation inside the washcoat can be neglected. More detailed numerical simulations, where the mass balances over the washcoat were explicitly taken into account, confirmed this.[36] These calculations also indicated that external mass- and heat transfer limitations could be neglected. Figure 5 shows the CO conversion as a function of the temperature. For these conditions the reaction reaches thermodynamic equilibrium at temperatures above 300°C. In Figure 6 the CO conversion is plotted as a

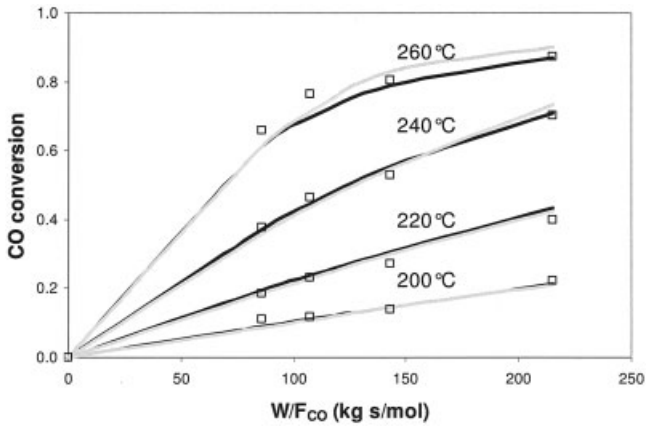

Figure 6. CO conversion as a function of W/F_{CO} at different temperatures.

P_{CO} = 0.1 bar, P_{H2O} = 0.2 bar, P_{H2} = 0.3 bar, P_{CO2} = 0.1 bar, balanced in argon. (symbols: experimental data, gray line: rate Eq. 6, black line: rate Eq. 9).

Table 2. Rate and Sorption Constants and Activation Energy with their 95% Confidence Intervals Estimated on the Basis of Rate Eq. 8

N_sA (mol/kg$_{cat}$s)	K_{CO}	K_{H2O}	K_{H2}	K_{CO2}	E_{act} (kJ/mol)
$3.7 \pm 2.6\ 10^7$	94.4 ± 74	12.2 ± 4.3	462 ± 344	2.4 ± 1.4	78.2 ± 2

function of W/F_{CO} at different temperatures. Although deactivation of Pt/ceria catalysts has been reported in several studies,[10, 42 - 44] it has not been observed on the time scale of the kinetic experiments as the reproducibility of the experiments was within the estimated experimental error.

Modeling

The data have been initially modeled by a power law rate equation

$$r_{CO} = (4.3 \pm 2)10^5 \exp\left(\frac{-(76.8 \pm 2)10^3}{RT}\right) \times P_{CO}^{(0.13\pm0.1)} P_{H_2O}^{(0.49\pm0.1)} P_{H_2}^{(-0.45\pm0.05)} P_{CO_2}^{(-0.12\pm0.05)}(1-\beta) \quad (6)$$

where β is the reversibility factor

$$\beta = \frac{P_{CO_2}P_{H_2}}{K_{eq}P_{CO}P_{H_2O}} \quad (7)$$

where K_{eq} is the equilibrium constant for the overall WGS reaction. The correlation for K_{eq} proposed by Moe[45] has been used

$$K_{eq} = \exp\left(\frac{4577.8}{T} - 4.33\right) \quad (8)$$

Equation 6 gives the values of the estimated rate constant, reaction orders and apparent activation energy with their 95% confidence intervals. The confidence interval on the reaction order for CO is rather large. This is due to the strong correlation with the rate constant ($\rho = 0.92$). The full grey lines in Figures 5 and 6 are the conversions calculated with rate in Eq. 6.

Different rate equations based on Langmuir — Hinshelwood type mechanisms and redox mechanisms have been tested in the regression analysis of the experimental data. The following rate equation describes the data best

$$r_{CO} = \frac{k_{rds}K_{CO}K_{H_2O}P_{CO}P_{H_2O}(1-\beta)}{(1 + K_{CO}P_{CO} + \sqrt{K_{H_2}P_{H_2}})^2(1 + \sqrt{K_{H_2O}P_{H_2O}} + K_{CO_2}P_{CO_2})} \quad (9)$$

The rate constant has been expressed in a reparametrized form of the Arrhenius equation to account for the temperature dependence of the reaction rate and to diminish the correlation between the preexponential factor and the activation energy. The K_i's are adsorption equilibrium constants. In the regression analysis no Van 't Hoff temperature dependence of these constants has been taken into account. The activation energies are, therefore, all apparent energies. The partial pressures are expressed in bars.

The adsorption enthalpies of the adsorbed species could not be estimated correctly due to the strong correlation with the other parameters. The parameter estimates corresponding to rate Eq. 9 are tabulated in Table 2 together with their 95% confidence intervals. Although the confidence intervals on some of the parameters are rather large they are all statistically significant. Removing one of the equilibrium constants from the rate equation results in a worse fit. The full black lines in Figures 5 and 6 are the conversions calculated with rate Eq. 9. A parity plot shown in Figure 7, also illustrates the good agreement between all the calculated conversions for both the power law equation, as well as the L-H expression and the experimental data. Both models describe the data equally well. No systematic deviations are observed for both models.

Discussion

The reaction order of CO is close to zero, indicating that the active sites for CO adsorption are close to saturation. The reaction orders of the products indicate that the reaction is inhibited by hydrogen and to a lesser extent by carbon dioxide. Hilaire et al. observed similar reaction orders over a Pd/ceria catalyst.[14] They measured a lower activation energy of 38 kJ/mol. The apparent activation energy obtained with rate Eqs 6 and 9 amounts around 78 kJ/mol. These values are slightly lower than the one reported by Wheeler et al.[21] of 80 kJ/mol, and the one reported by Panagiotopoulou and Kondarides[46] of 89 kJ/mol both for a Pt/ceria catalyst.

Different models are put forward in the literature to explain the increased activity of platinum ceria catalysts both for the oxidation of CO as for the water-gas shift reaction. On the one hand a mechanism is proposed where the active site is located on the ceria and the role of platinum is that of a promoter.[11-13] This reaction mechanism involves formate species as intermediates.

On the other hand, some studies locate the actives sites at the metal-ceria interface with the metal directly participating in the

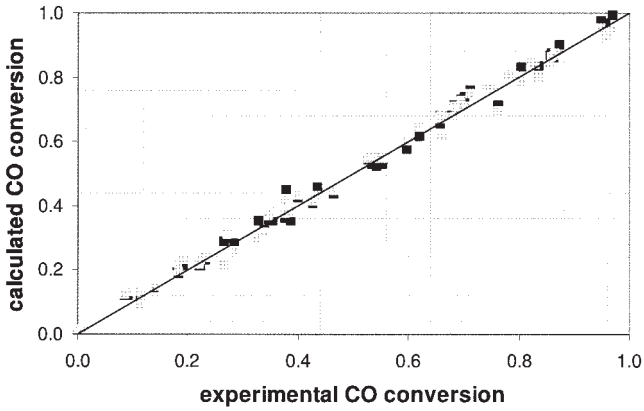

Figure 7. Parity plot of all data.

For conditions see Table 1. (calculated CO conversions given by: gray symbols rate Eq. 6, black symbols rate Eq. 9).

reaction mechanism.[9, 16] The rate enhancement is explained by either an increased oxygen mobility or by the creation of an additional site for either oxygen or water adsorption. The latter explanation seems to fit best with our observations. It is substantiated by the fact that the data are best described by a dual site mechanism, an activation energy in the range of those reported for the water-gas shift reaction over Pt/alumina catalysts and the zero reaction-order of CO, typical of reactions of CO over Pt.

Based on the arguments given above on both the role of platinum and ceria and knowing that a free platinum appears in the rate-determining step the following mechanism is put forward

$$CO + * \rightleftarrows CO* \quad (10)$$

$$H_2O + Ce{-}O \rightleftarrows HO{-}Ce{-}OH \quad (11)$$

$$CO* + HO{-}Ce{-}OH \rightleftarrows COOH* + Ce{-}OH \quad (12)$$

$$COOH* + Ce{-}OH + * \rightleftarrows 2H* + Ce{-}O{-}CO_2 \quad (13)$$

$$2H* \rightleftarrows H_2 + 2* \quad (14)$$

$$Ce{-}O{-}CO_2 \rightleftarrows CO_2 + Ce{-}O \quad (15)$$

Carbon monoxide adsorbs reversibly on platinum (Eq. 10), and water adsorbs dissociatively on (partially reduced) ceria (Eq. 11). Carboxyl formation takes place via the reaction of adsorbed CO with a hydroxyl group on the ceria (Eq. 12). The rate-determining step (Eq. 13) is the reaction between the carboxyl species, and the second hydroxyl group on the ceria into adsorbed hydrogen and carbon dioxide. Once an adjacent platinum site becomes free this carboxyl complex decomposes into the reaction products. Hydrogen competes with carbon monoxide for platinum adsorption sites and is therefore included in the denominator (Eq. 14). Similarly, carbon dioxide adsorbs strongly on ceria (Eq. 15).

The reaction steps involving carboxyl species on platinum all have preexponential factors of approximately 10^{11} s^{-1} [47]. The modeling resulted in the estimation of the product of the preexponential factor and the number of active sites. Due to the uncertainty on the number of active sites, the estimated value of the pre-exponential of the rate-determining step lies in the range between 10^{10}–10^{12} s^{-1}, thus, in good agreement with theory The equilibrium constants for CO and H_2 chemisorption on platinum in the temperature range of 200 – 400 °C are in the range of 2 10^3 –2 bar^{-1}, and 2 10^3 –20 bar^{-1}, respectively.[20, 48] The value estimated for both the CO and the H_2 adsorption equilibrium (Table 2) constants fall well within this range. The estimated value of the adsorption equilibrium constant for CO_2 on ceria (Table 2) agrees very well with the values measured by Nibbelke et al.[49], which are in the range of 4 –2 bar^{-1} for temperatures between 200 – 400 °C. The good agreement of the values of the rate constant and the adsorption equilibrium constants with data from other studies reinforces the physical validity of the model.

Conclusions

Microreactors may be used advantageously as a kinetic device, when proper hydrodynamic conditions are fulfilled. Long platelets rather than a stack of short platelets favor these conditions. The main advantages of microstructured reactors for kinetic studies is the use of very thin catalyst films that minimize internal diffusion limitations and the good thermal characteristics of stainless steel structures leading to improved isothermal conditions.

A kinetic study using a microstructured reactor has been performed for the water-gas shift reaction over a platinum/ceria/alumina catalyst. The use of the microstructured reactor, rather than a packed-bed reactor, has allowed measuring the intrinsic kinetics. The reaction conditions cover a wide range of the operating variables. Rate equations based on different reaction mechanisms have been used for the regression of the experimental data. The reaction rate is almost zero-order in carbon monoxide and strongly inhibited by the partial pressure of hydrogen, and to a lesser extent by that of carbon dioxide. The rate equation that fits the data best is based on a dual-site mechanism with a rate-determining step that involves a species adsorbed on platinum, a species adsorbed on ceria and a free platinum site. Based on this observation a reaction mechanism has been proposed where carbon monoxide, adsorbed on platinum, reacts with water, dissociatively chemisorbed on ceria, to yield a carboxyl species as an intermediate. This carboxyl species reacts with a second hydroxyl group and decomposes over a free platinum site into carbon dioxide and hydrogen. The corresponding rate equation is based on physically meaningful parameters.

Acknowledgments

Part of this work has been funded by the EU "MINIREF" project (NNE5-2001-00056). IMM - Institut für Mikrotechnik Mainz GmbH is gratefully acknowledged for providing the microstructured platelets. The authors wish to thank C. Mirodatos for many fruitful discussions, M. Aouine for the TEM analysis, A. Giroir-Fendler, L. Retailleau, and S. Benard for the hydrogen chemisorption measurements.

Notation

A = preexponential factor, s^{-1}
C_m = dimensionless mixing-cup concentration
$\mathring{d}_{Pt}$ = surface area average diameter of the platinum particles, nm
d_t = tube diameter, m
D = molecular-diffusion coefficient, m^2/s
D_{Aris} = dispersion coefficient, m^2/s
D_{Pt} = platinum dispersion
D_{reac} = dispersion coefficient in the presence of reaction, m^2/s
E_{act} = activation energy, kJ/mol
F_{CO} = molar flow rate of CO, mol/s
k'_{rds} = rate coefficient of the rate-determining step (includes number of active sites), $mol/bar^2/kg_{cat}/s$
K_i = adsorption equilibrium constant for species i, 1/bar
K_{eq} = overall equilibrium constant
L = reactor length, m
N_s = number of active sites, mol/kg_{cat}
P_i = partial pressure of component i, bar
r_{CO} = rate of CO disappearance, $mol/kg_{cat}/s$
$R'(C_m)$ = derivative with respect to the rate R
T = temperature, K
u = gas velocity, m/s
W = catalyst mass, kg
β = reversibility factor
ρ = correlation coefficient

Literature Cited

1. De Bruijn FA. The current status of fuel cell technology for mobile and stationary applications. *Green Chem.* 2005;7(3):132-150.
2. Ruettinger W, Ilinich O, Farrauto RJ. A new generation of water gas

shift catalysts for fuel cell applications. *J Power Sources.* 2003;118: 61-65.
3. Schlatter JC, Mitchell PJ. Three-way catalyst response to transients. *Ind Eng. Chem Prod Res Dev.* 1980;19(3) :288-293.
4. Kim G. Ceria-promoted three-way catalysts for auto exhaust emission control. *Ind Eng Chem Prod Res Dev.* 1982;21:267-274.
5. Herz RK, Sell JA. Dynamic behavior of automotive catalysts. III. Transient enhancement of water-gas shift over rhodium. *J Catal.* 1985;94:166-174.
6. Mendelovici L, Steinberg M. Methanation and water-gas shift reactions over Pt/CeO2. *J Catal.* 1985;96:285-287.
7. Barbier Jr J, Duprez D. Reactivity of steam in exhaust gas catalysis. I. Steam and oxygen/steam conversions of carbon monoxide and of propane over PtRh catalysts. *Appl Catal B.* 1993;3:61-83.
8. Whittington BI, Jiang CJ, Trimm DL. Vehicle exhaust catalysis: I. The relative importance of catalytic oxidation, steam reforming and water-gas shift reactions. *Catal Today.* 1995;26:41-45.
9. Bunluesin T, Gorte RJ, Graham GW. Studies of the water-gas-shift reaction on ceria-supported Pt, Pd, and Rh: Implications for oxygen-storage properties. *Appl Catal B.* 1998;15:107-114.
10. Ghenciu AF. Review of fuel processing catalysts for hydrogen production in PEM fuel cell systems. *Current Opinion Solid State Mater Sci.* 2002;6(5):389-399.
11. Shido T, Iwasawa Y. Reactant-Promoted Reaction Mechanism for Water-Gas Shift Reaction on Rh-Doped CeO_2. *J Catal.* 1993;141:71-81.
12. Jacobs G, Williams L, Graham UM, Sparks DE, Thomas G, Davis BH. Low temperature water gas shift: *in situ* DRIFTS-reaction study of ceria surface area on the evolution of formates on Pt/CeO_2 fuel processing catalysts for fuel cell applications. *Appl Catal A.* 2003;252: 107-118.
13. Jacobs G, Patterson PM, Graham UM, Crawford AC, Davis BH. Low temperature water gas shift: the link between the catalysis of WGS and formic acid decomposition over Pt/ceria. *Int J Hydrogen Energy.* 2005;30:1265-1276.
14. Hilaire S, Wang X, Luo T, Gorte, RJ, Wagner J. A comparative study of water-gas shift reaction over ceria-supported metallic catalysts. *Appl Catal A.* 2004;258:271-276.
15. Tibiletti D, Goguet A, Meunier FC, Breen JP, Burch R. On the importance of steady-state isotopic techniques for the investigation of the mechanism of the reverse water-gas-shift reaction. *Chem Commun.* 2004:1636-1637.
16. Goguet A, Meunier FC, Tibiletti D, Breen JP, Burch R. Spectrokinetic investigation of reverse water-gas-shift reaction intermediates over a Pt/CeO_2 catalyst. *J Phys Chem B.* 2004;108:20240-20246.
17. Jacobs G, Davis BH. Reverse water-gas shift reaction: steady state isotope switching study of the reverse water-gas shift reaction using in situ DRIFTS and a Pt/ceria catalyst. *Appl Catal A.* 2005;284:31-38.
18. Lam CW, Stacey MS, Trimm DL. The combustion of methane on platinum-alumina fibre catalysts III The kinetics of the water gas shift reaction. *Chem Eng Sci.* 1981;36:226-228.
19. Grenoble DC, Estadt MM, Ollis DF. The Chemistry and Catalysis of the Water Gas Shift Reaction. 1. The kinetics over Supported Metal Catalysts. *J Catal.* 1981;67:90-102.
20. Mhadeshwar AB, Vlachos DG. Is the water-gas shift reaction on Pt simple? Computer-aided microkinetic model reduction, lumped rate expression, and rate-determining step. *Catal Today.* 2005;105:162-172.
21. Wheeler C, Jhalani A, Klein EJ, Tummala S, Schmidt LD. The water-gas shift reaction at short contact times. *J Catal.* 2004;223:191-199.
22. Ehrfeld W, Hessel V, Loewe H. Microreactors. Weinheim: Wiley-VCH, 2000.
23. Rebrov EV, de Croon MHJM, Schouten JC. Development of the kinetic model of platinum catalyzed ammonia oxidation in a microreactor. *Chem Eng J.* 2002;90:61-76.
24. Ouyang, Bednarova L, Besser RS, Ho P. Preferential oxidation (PrOx) in a thin-film catalytic microreactor: Advantages and limitations. *AIChE J.* 2005;51(6):1758-1172.
25. Perrichon V, Retailleau L, Bazin P, Daturi M, Lavalley JC. Metal dispersion of CeO_2-ZrO_2 supported platinum catalysts measured by H_2 or CO chemisorption. *Appl. Catal. A.* 2004;260:1-8.
26. Froment GF, Bischoff K. Chemical Reactor Analysis and Design. 2nd ed. New York: Wiley;1990.
27. Hindmarsh AC. ODEPACK, A Systematized Collection of ODE Solvers. Amsterdam: Elsevier; 1983.
28. Levenberg K. A method for the solution of certain non-linear problems in least squares. *Q Appl Math.* 1944;11:164-168.
29. Marquardt DW. An algorithm for least squares estimation of non-linear parameters. *J Soc Ind Appl Math.* 1963;11:431-441.
30. Froment GF, Hosten LH. Catalytic Kinetics: *Modelling. Catalysis Science and Technology*. Anderson JR, Boudart M. Eds. Springer Verlag: Berlin; 1981.
31. Aris R. On the dispersion of a solute in a fluid flowing through a tube. *Proc R. Soc Lond Ser. A* 1956;235:67-77.
32. Levenspiel O. *Chemical Reaction Engineering*. 3rd Ed. New York: Wiley;1999.
33. Chakraborty S, Balakotaiah V. Low-dimensional models for describing mixing effects in laminar flow tubular reactors. *Chem Eng Sci.* 2002;57:2545-2564.
34. Fuller EN; Schettler PD, Giddings JC. A new method for prediction of binary gas-phase diffusion coefficients. *J Ind Eng Chem.* 1966;8(5):8-27.
35. Delsman ER, de Croon MHJM, Elzinga GD, Cobden PD, Kramer GJ, Schouten JC. The influence of differences between microchannels on microreactor performance. *Chem Eng Tech.* 2005;28:367-375.
36. Germani G, Alphonse P, Courty M, Schuurman Y, Mirodatos C. Platinum/ceria/alumina catalysts on microstructures for carbon monoxide conversion. *Catal Today.* 2005;110:114-120.
37. Hayes RE, Kolaczkowski ST. *Introduction to Catalytic Combustion*. Gordon and Breach Science Publishers; 1997.
38. Scholten JJF, Pijpers AP, Hustings AML. Surface characterization of supported and nonsupported hydrogenation catalysts. *Catal Rev Sci Eng.* 1985;27(1) :151-206.
39. Yasaki S, Yoshino Y, Ihara K, Ohkubo K, US Patent No. 5,208,206, May 4; 1993.
40. Valentini M, Groppi G, Cristiani C, Levi M, Tronconi E, Forzatti P. The deposition of γ-Al_2O_3 layers on ceramic and metallic supports for the preparation of structured catalysts. *Catal Today.* 2001;69:307-314.
41. Satterfield, CN. *Mass Transfer in Heterogeneous Catalysis*. Robert E Krieger Publishing Company; 1981.
42. Zalc JM, Sokolovskii V, Löffler DG. Are noble metal-based water-gas shift catalysts pratical for automotive fuel processing? *J Catal.* 2002; 206:169-171.
43. Wang X, Gorte RJ, Wagner JP. Deactivation mechanisms for Pd/Ceria during the water-gas shift reaction. *J Catal.* 2002;212:225.230.
44. Goguet A, Meunier FC, Breen JP, Burch R, Petch MI, Ghenciu AF. Study of the origin of the deactivation of a Pt/CeO_2 catalyst during reverse water gas shift (RWGS) reaction. *J Catal.* 2004;226:382-392.
45. Moe, JM. Design of water-gas shift reactors. *Chem Eng Progr.* 1962; 58:33-36.
46. Panagiotopoulou PC, Kondarides DI. Effects of Physicochemical and Morphological Properties of Supported Noble Metal Catalysts on their Activity for the Water-Gas Shift Reaction. 13th *international congress on catalysis* Paris; 2004.
47. Mhadeshwar AB, Vlachos DG. Microkinetic modeling for water-promoted CO oxidation, water-gas shift, and preferential oxidation of CO on Pt. *J Phys Chem B.* 2004;108:15246 - 15258.
48. Herz RK, Marin SP. Surface chemistry models of carbon monoxide oxidation on supported platinum catalysts. *J Catal.* 1980;65:281-296.
49. Nibbelke RH, Nievergeld AJL, Hoebink JHBJ, Marin GB. Development of a transient kinetic model for the CO oxidation by O_2 over a $Pt/Rh/CeO_2/\gamma$-Al_2O_3 three-way catalyst. *Appl Catal B.* 1998;19:245-259.

Manuscript received Sept. 27, 2005, and revision received Nov. 22, 2005.